Modeling biogeochemical processes in subterranean estuaries: The effect of flow dynamics and redox conditions on submarine groundwater discharge

Claudette Spiteri, Caroline P. Slomp, Kagan Tuncay and Christof Meile

Abstract **A 2D density dependent reactive transport model is used to investigate the fate of nutrients (NO_3^-, NH_4^+ and PO_4) in idealized subterranean estuaries, representing four endmembers of oxic/anoxic aquifer and seawater redox conditions. The flow dynamics in a coastal aquifer are coupled with a reaction network, which takes into account some of the main biogeochemical pathways that remove/transform nutrients. The extent of groundwater nutrient removal prior to discharge into coastal waters and the resulting input of nitrogen and phosphorus species is largely determined by the prevalent flow characteristics and redox conditions in the freshwater seawater mixing zone. Denitrification, the key NO_3^- removing process, prevails under anoxic conditions, resulting in dissolved inorganic nitrogen to phosphorus ratios (N:P ratios) of submarine groundwater discharge lower than that of dissolved organic matter (DOM). Both low fluid flow rates and high DOM reactivity enhance the depletion of NO_3^- through denitrification. On the other hand, extremely high N:P ratios are predicted when anoxic groundwater meets oxic seawater, due to the localized P retention onto the $Fe(OH)_3$ that precipitate along the redox interface. Due to the occurrence of coupled nitrification denitrification, the position of the NO_3^- and NH_4^+/PO_4 plumes, relative to the water table, is reversed compared to their original positions at the landward source.**

Index Terms **submarine groundwater discharge, subterranean estuaries, nutrients, nitrogen, phosphorus, reactive transport modeling**

Manuscript received September, 2006. CM acknowledges support by Georgia Sea Grant of the National Sea Grant College Program of the U.S. Department of Commerce's National Oceanic and Atmospheric Administration under NOAA Grant #NA04OAR4170033. The views herein do not necessarily reflect the views of any of those organizations. CPS was supported by the Royal Netherlands Academy of Arts and Sciences and the Netherlands Organisation for Scientific Research (VIDI-grant).

C. Spiteri and C.P. Slomp are with the Department of Earth Sciences Geochemistry, Faculty of Geosciences, Utrecht University, P.O. Box 80021, 3508 TA Utrecht, The Netherlands (corresponding author C.Spiteri: +31-30-253-4968; fax: +31-30-253-5302; e-mail: c.spiteri@ geo.uu.nl; slomp@geo.uu nl).

K. Tuncay is with the Department of Chemistry, Indiana University, Bloomington, IN 47405, USA (e-mail: ktuncay@indiana.edu).

C Meile is with the Department of Marine Sciences University of Georgia, Athens, GA 30602-3636, USA (e-mail: cmeile@uga.edu).

I. Introduction

Submarine groundwater discharge (SGD) is an important transport pathway for a variety of dissolved chemical species such as nutrients, heavy metals, radionuclides and organic compounds from land to coastal waters [1]. Although in most areas SGD rates are generally low compared to riverine inputs (worldwide range of 0.03 to 454 m yr^{-1}, most of which fall below 36 m yr^{-1} and may consist of both freshwater and recirculated seawater; [2]), the high concentration of nutrients in freshwater SGD can significantly contribute "new" nutrients to the coastal zone, especially in areas strongly influenced by human activities. The discharge of nitrogen (N) and phosphorus (P)-contaminated groundwater, commonly originating from fertilizer/manure leachates and waste-water from septic systems, can trigger eutrophication and the growth of nuisance algal blooms, causing the degradation of coastal environments [3].

Most studies to date have focused on the identification of SGD hotspots and quantification of SGD rates [4]-[6]. However, the chemical composition of SGD is not only affected by the landward freshwater sources and discharge rates, but also by the reactions within the subterranean estuaries, the mixing zone of freshwater and seawater in coastal aquifers [7]. Nutrient dynamics in these coastal mixing zones, and hence SGD of nutrients, are strongly determined by the redox characteristics of freshwater and seawater ([8]-[12]). For this reason, redox processes in coastal aquifers, particularly within the subterranean estuaries, are now receiving more attention, although detailed studies on the biogeochemistry are still very limited.

In a review on nutrient inputs to the coastal ocean through SGD, [2] presented four hypothetical conceptual models which illustrate the fate of nutrients (NO_3^-, NH_4^+, PO_4) in subterranean estuaries characterized by different redox conditions:

Case 1): oxic groundwater meeting oxic seawater
Case 2): oxic groundwater meeting anoxic seawater
Case 3): anoxic groundwater meeting oxic seawater
Case 4): anoxic groundwater meeting anoxic seawater

For each case, the authors discussed the effect of the prevailing biogeochemical reactions on the discharge of N and P. Here, we use a 2D density-dependent reactive transport model to simulate the water flow and biogeochemical processes affecting N and P in the four scenarios outlined above, using a model coastal aquifer with a typical freshwater/seawater wedge. The fresh groundwater is assumed to be contaminated with a $NO_3^-/NH_4^+/PO_4$ plume, which typically originates from sewage effluents or agriculture activities along the coast. We first perform four baseline simulations to assess the impact of prevalent redox conditions on nutrient distributions and the subsequent dissolved inorganic nitrogen to phosphorus ratios (N:P ratios) of the freshwater and recirculated components of SGD. Then we extend our study to test the effect of a) higher transverse dispersivity (α_T) on the N:P ratios of SGD in Case 1, b) additional NO_3^- removal through denitrification with Fe^{2+} as electron-donor in the oxic/anoxic redox interface of Case 2, c) higher freshwater discharge rates and d) higher DOM reactivity on NO_3^- removal through denitrification in Case 3.

II. Model Setup

A schematic diagram of the rectangular model domain, representing a 60 m x 20 m confined aquifer, including the set of typical aquifer parameters used in the simulations, is given in Fig. 1.

The list of chemical constituents included in the model are NO_3^-, NH_4^+, PO_4, $PO_{4(ads)}$(s), O_2, DOM, Fe^{2+}, $Fe(OH)_3$(s) and Ca^{2+} and salt. Table 1 provides the concentrations in the different parts of the aquifers assumed in the four scenarios. In each case, the aquifer is contaminated by a freshwater NO_3^-, NH_4^+ or PO_4 plume of constant composition, depending on the groundwater redox conditions. Both oxic and anoxic aquifers are considered to be impacted by a NO_3^- plume. Anoxic aquifers (Cases 3 and 4) contain NH_4^+, while in the scenarios with oxic groundwater (Cases 1 and 2), it is assumed that the NH_4^+ plume has been converted to NO_3^-. A PO_4 plume is considered in all cases, but with a much lower concentration in the oxic groundwater (Cases 1 and 2). The extended reaction network, comprising 6 kinetic reactions, is given in Table 2, while Table 3 contains the list of reaction parameter values. The rate laws for dissolved organic matter (DOM) degradation (Table 2) allow a smooth transition from aerobic degradation to denitrification to $Fe(OH)_3$ reduction, assuming a first order rate with respect to the electron donor, DOM, and a pseudo Michaelis-Menton type relationship with respect to the electron acceptor [13]. Nitrification, Fe^{2+} reoxidation and Fe^{2+} denitrification are described by bimolecular rate laws. PO_4 removal is assumed to occur through adsorption of dissolved PO_4, leading to the instantaneous redistribution of total PO_4 into dissolved and sorbed P, $PO_{4(ads)}$. Sorption is represented by a sorption isotherm, in which the adsorption coefficient (K_d) is a function of the concentration of $Fe(OH)_3$

$$K \cdot Fe(OH)_3 \cdot \frac{\varphi}{(1-\varphi)} = \frac{[PO_{4(ads)}]}{[PO_{4(aq)}]} \qquad (1)$$

i.e. $K_d = K*Fe(OH)_3$. The effects of variations in ionic strength and temperature between the freshwater and seawater are neglected.

Model calculations are performed for a saturated porous medium, using the classical Darcy flow approximation. In each time step, the pressure field is first calculated, taking into account density variations as a linear function of salinity. From the calculated pressure field, the velocity field is derived using the Darcy law, and the anisotropic dispersion tensor is obtained for the given longitudinal and transverse dispersivities [14]. Concentration fields are then computed by solving mass conservation equations for all species, considering diffusive/dispersive and advective transport for solutes. Reaction rates are evaluated from the previous concentration field for both solids and solutes (Table 2). We use a Galerkin finite element formulation for spatial discretization and a conjugate gradient approach to solve the linear set of equations at each time step [15], [16]. Boundary and initial conditions for the simulations are provided in Fig. 1 and Table 1.

III. Results

A. Baseline Simulations

Fig. 2 shows the steady-state salt wedge and SGD velocities at the seaward boundary (60 m) representing average flow conditions, not taking into account the effect of tidal pumping or seasonal variation in freshwater discharge. Concentration distributions for NO_3^-, NH_4^+ and PO_4 for Cases 1-4 at steady-state are shown in Fig. 3. A set of analogous simulations are also performed in which all reactions are turned off, referred to as the "conservative" runs. For comparison, Fig. 4 shows the concentration profiles of the most important solute species at the seaward boundary, together with their respective "conservative" ones.

Due to the absence of reactive DOM (Table 1), the results for the completely oxic model subterranean estuary show very limited transformation or removal of all species, Case 1 (Figs. 3a-c, 4a-e). The propagation of the NO_3^- plume towards the sea is virtually conservative. A drop in the peak discharge concentration relative to the source concentration is observed due to dispersion. The concentrations of NH_4^+ and PO_4 are relatively low, even though PO_4 removal through adsorption is not possible, since no "in situ" formation of $Fe(OH)_3$ occurs.

The trend in the NH_4^+ profile in the oxic groundwater/anoxic seawater case, Case 2 (Fig. 4g), indicates a redistribution relative to the "conservative" profile, resulting in lower concentrations in the freshwater part due to nitrification and higher concentrations in the seawater as a result of DOM degradation. The NH_4^+ transported in the anoxic seawater is nitrified to NO_3^-, slightly increasing the NO_3^- concentrations along the interface (Fig. 4f).

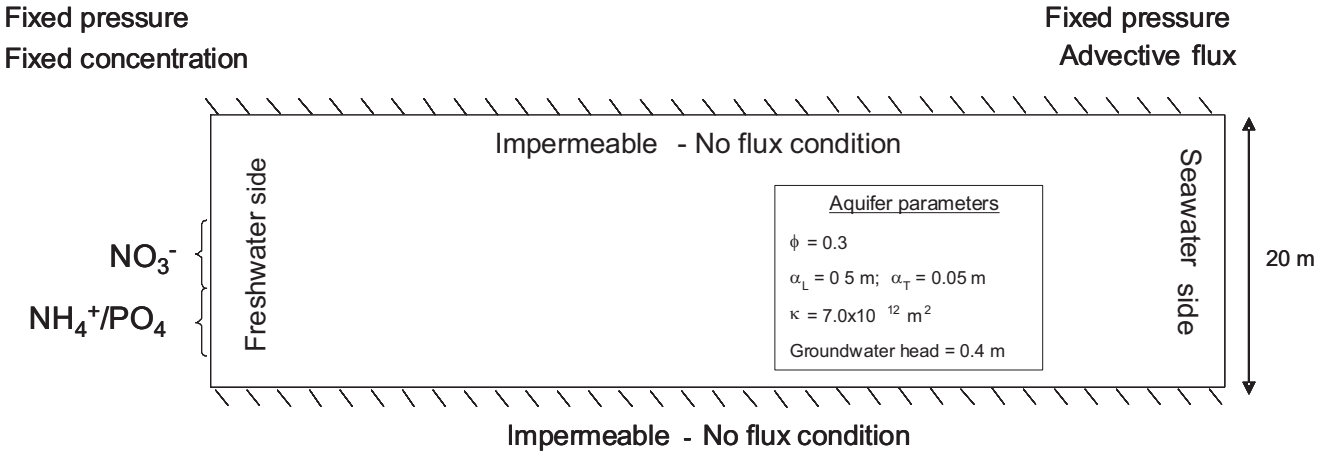

Fig. 1. Schematic diagram of the model setup, showing the model domain, boundary conditions, aquifer parameters used in the baseline simulations and depths of the nutrient source plumes

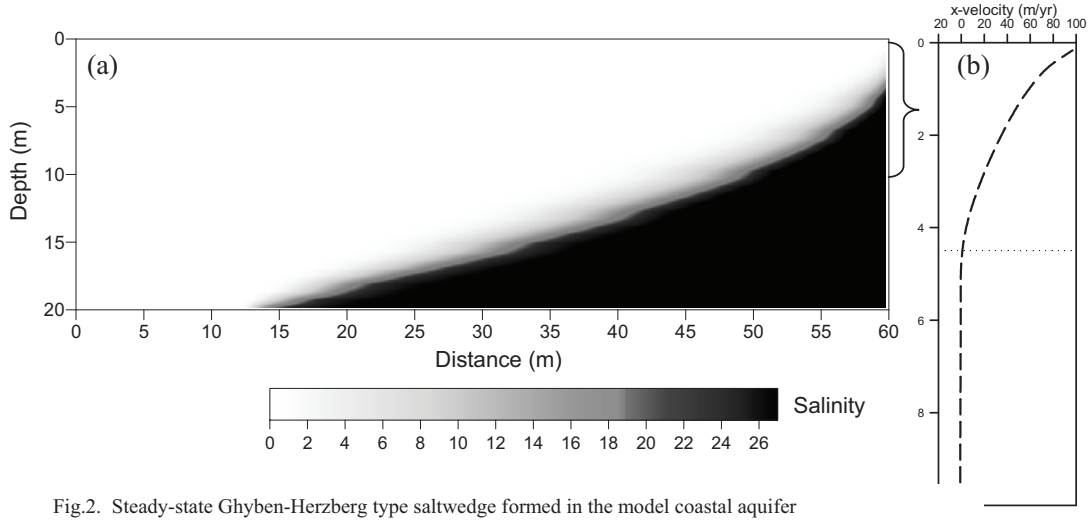

Fig.2. Steady-state Ghyben-Herzberg type saltwedge formed in the model coastal aquifer

TABLE 1
CONCENTRATIONS OF THE DIFFERENT SPECIES ASSUMED IN THE FOUR SCENARIOS. CONCENTRATIONS IN THE GROUNDWATER ARE FIXED AT THE LANDWARD BOUNDARY OR AS PLUMES**; THOSE IN THE SEAWATER ARE USED AS INFLOWING WATER COMPOSITION OF THE SALT WEDGE AT THE OCEAN BOUNDARY. INITIAL CONCENTRATIONS ARE SET TO 0.

Species *	Concentration in oxic groundwater	Concentration in anoxic groundwater	Concentration in oxic seawater	Concentration in anoxic seawater
NO_3	0.25 (a)**	0.25 (a) **	0.02 (b)	-
NH_4^+	-	0.2 (c) **	0.001 (b)	0.01 (c)
PO_4	0.001 (a) **	0.05 (a)**	0.001 (b)	0.3 (c)
$PO_{4(ads)}$ (s)	-	-	-	-
O_2	0.05 (a)	0.0	0.2 (b)	0.0
DOM	-	0.75 (c)	-	0.33 (c)
Fe^{2+}	-	0.1 (d)	-	0.1 (d)
$Fe(OH)_3$ (s)	-	-	-	-
Ca^{2+}	-	1.0 (c)	10.5 (b)	6.7 (c)
Salt	0.28 (d)	0.28 (d)	27.0 (d)	27.0 (d)

(a) [2]; (b) [23]; (c) [12]; (d) [24]
(-) low concentrations, assumed to be 0
* units for solutes are in mmol dm^3 pore water, denoted as mM; solids (s) are in mmol dm^3 solid, denoted as mmol dm^3; units for salt are ‰.

However, the net removal of NO_3^- is only marginal, mainly because denitrification is hindered by the presence of O_2 in the oxic groundwater. These results are in qualitative agreement with field observations by Uchiyama and co-workers [9] who report the occurrence of high NO_3^- concentrations near the shore of Hasaki Beach in Japan, which they attribute to nitrification in the inland aerobic aquifer. Towards the shoreline, dissolved N in the freshwater part mixes with N supplied from the mineralization of organic matter from the seabottom, analogous to our modeled NH_4^+-rich seawater endmember. A net removal of modeled PO_4 is observed since PO_4 is absorbed on the iron oxides that form on the oxic/anoxic interface. This results in the retention and restricted landward penetration of the seawater PO_4 front (Fig. 3f).

The nutrient distributions and species profiles obtained in Case 3, where anoxic groundwater meets oxic seawater, are given in Fig. 3g-i and Fig. 4k-o. Here, significant NO_3^- removal through denitrification is observed in the anoxic aquifer (Fig 3g), which however, is not enough to consume the DOM completely (Fig. 4o). This implies that denitrification is either limited by the low reactivity of the DOM or by the high water flow velocity. Comparison of the NO_3^- and NH_4^+ profiles with the "conservative" ones indicate the occurrence of coupled nitrification-denitrification at the redox interface. Denitrification lowers the peak NO_3^- concentration from ~0.06 mM to ~ 0.02 mM at a depth of 1 m, while a new NO_3^- peak develops at a depth of ~3 m as a result of nitrification. The upward shift in the NH_4^+ plume also reflects the occurrence of coupled nitrification-denitrification, with a depletion of NH_4^+ at a depth of ~ 3m and production at ~ 1m. It is interesting to note that, as a result of coupled nitrification-denitrification and PO_4 adsorption, the depths of the NO_3^- and NH_4^+/PO_4 peaks at the seaward boundary are reversed relative to their original position at the landward source side. The PO_4 plume is attenuated through sorption to concentrations as low as 0.005 mM prior to discharge. Such a phenomenon occurs in the subterranean estuary of Waquoit Bay, MA, where the formation of an "Iron Curtain" scavenges the freshwater PO_4 prior to discharge into the coastal zone [10], [17]. The freshwater NO_3^- at the same site travels as a plume and apparently discharges to the bay within the intertidal zone [18] without major denitrification, possibly due to the lack of labile DOM or high water flow rates.

In a completely anoxic subterranean estuary, Fig. 3j-l and Fig. 4p-t, most of the anthropogenic NO_3^- is consumed, causing the plume maximum to drop from ~ 0.05 mM to 0.01 mM in the anoxic groundwater. Yet, the shape of the profile is distinct from Case 3, since there is no additional NO_3^- production from nitrification. Our model postulates an increase in the NH_4^+ peak due to DOM degradation, but virtually no PO_4 removal due to the absence of $Fe(OH)_3$. Nevertheless, the calculated saturation indices for hydroxyapatite, assuming a constant pH of 7.0 (not shown) indicate that PO_4 removal through hydroxyapatite precipitation may play a role, especially in carbonate aquifers. This was reported for an anoxic, saline Floridian aquifer where almost complete removal of dissolved wastewater phosphorus through the formation crystalline calcium phosphate occurs [19].

The overall effect of the reactions on N and P inputs into the coastal ocean via SGD is illustrated in Fig. 5a-d, which shows the N:P profiles at the seawater boundary compared to the corresponding "conservative" ones. The N:P ratio of SGD in Case 1 decreases from a maximum of 600 in the freshwater part, down to ~ 20 in the recirculated SGD, representing the marine endmember (Table 1, Fig. 5a) These relatively high values of N:P ratios (greater than twice the N:P ratio on the landward domain boundary) in the freshwater discharge zone are the result of the converging flow in the freshwater part, rather than of reaction. Comparison of the N:P profile obtained in Case 2 with the "conservative" counterpart shows an significant increase in the N:P ratio of the freshwater SGD due to PO_4 adsorption (Fig. 5b). Nitrification has no major effect on the N:P ratios since it is merely the interconversion of N from one species, NH_4^+, to another NO_3^-. In Case 3 (Fig. 5c), the N:P of the freshwater SGD increases drastically primarily due to localized retention of PO_4 on $Fe(OH)_3$ at the interface. On the contrary, in Case 4, the N:P of SGD is close to the Redfield ratio due to the lack of PO_4 retention in the anoxic subterranean estuary. The N:P ratios for the four cases are plotted together in Fig. 5e, to highlight the variety in the possible range resulting from different redox conditions. Cases 1 and 4 show a smooth decline with depth, whereas the profiles in Cases 2 and 3 reflect localized sorption of PO_4.

B. Sensitivity Analysis

A sensitivity analysis is performed to investigate factors that are poorly known and are expected to have a significant impact on the baseline model results. We specifically focus on the role of dispersion, denitrification pathways, flow rate and DOM reactivity (Table 4). Doubling the value of α_T in Case 1, the most conservative scenario with minimal feedbacks to and from reactions, we observe a broadening of the freshwater-seawater interface, an increased overlap between the freshwater and seawater species and an increased transverse dispersion of the NO_3^- plume (Fig. 6a). The broadening of the NO_3^- plume alone causes a decrease in the maximum N:P ratio to ~400 (Fig. 6b).

An alternative pathway for NO_3^- reduction is its reaction with Fe^{2+} as an electron-donor. Although field evidence of NO_3^- reduction by Fe^{2+} has been presented by [20], the exact reaction mechanism is still not fully understood [21], [22]. However, the inclusion of Fe^{2+} denitrification, which is assumed to follow a bimolecular rate law in our model, leads to little additional NO_3^- removal (Fig. 7a). In contrast, the removal of PO_4 is enhanced substantially through sorption on the additional $Fe(OH)_3$ produced through the oxidation of Fe^{2+} (Fig. 7b, c).

Comparison of Fig. 8 a and b show that high groundwater flow rates reduce the efficiency of NO_3^- removal through denitrification from the core of the plume. As suggested by Capone and Slater [8], intermediate groundwater flow rates are a prerequisite for denitrification to occur. High rates will result in dominance of advective transport over reaction,

whereas low rates will limit denitrification due to a limited NO_3^- supply. The second sensitivity analysis run for Case 3, (Fig. 9) shows that the reactivity of the DOM is another important factor which determines the extent of NO_3^- removal. On increasing the rate of DOM degradation by one order of magnitude, near complete removal of NO_3^- is obtained close to its freshwater source (Fig. 9b).

IV. Conclusions

This study demonstrates that subterranean estuaries are biogeochemically active environments, characterized by complex nutrient dynamics. The results from the four baseline simulations show that the fate of N and P strongly depends on the redox conditions along the freshwater seawater continuum. However, the extent of freshwater and seawater mixing, assessed by changing the transverse dispersivity and flow rates, also plays a role on the degree of nutrient transformation/removal.

Denitrification and P sorption are the two key processes that determine the extent of nutrient removal. Denitrification is coupled not only to the reactivity of DOM, but also to the flow dynamics, since more efficient removal of NO_3^- is observed at lower rates of water flow. P sorption is mainly important in Cases 2 and 3, where a redox interface is formed when groundwater and seawater with different redox conditions interact. The overall effect of the various redox processes occurring within each subterranean estuary is reflected in the molar N:P ratio of the SGD. The different behaviors exhibited by N and P lead to a wide range of N:P ratios of SGD, spanning from ~0.03 to 30000**.**

References

[1] W. C. Burnett et al., "Quantifying submarine groundwater discharge in the coastal zone via multiple methods," *Science of the Total Environment*, vol. 367, pp. 498-593, 2006.

[2] C. P. Slomp, and P. Van Cappellen, "Nutrient inputs to the coastal ocean through submarine groundwater discharge: controls and potential impact," *Journal of Hydrology,* vol. 295, pp. 64-86, 2004.

[3] J. LaRoche et al., "Brown tide blooms in Long Island's coastal waters linked to interannual variability in groundwater flow," *Global Change Biology*, vol. 3, pp. 397-410, 1990.

[4] J. E Cable, W. C. Burnett, J. P. Chanton, and G. L. Weatherly, "Estimating groundwater discharge into the northeastern Gulf of Mexico using radon-222," *Earth and Planetary Science Letters*, vol. 144, pp 591-604, 1996.

[5] D. R. Corbett et al., "Patterns of groundwater discharge into the Florida Bay," *Limnology and Oceanography*, vol. 44, no. 4, pp. 1045-1055, 1999.

[6] J. Crusius et al., "Submarine groundwater discharge to a small estuary estimated from radon and salinity measurements and a box model," *Biogeosciences*, vol. 2, pp. 141-157, 2005.

[7] W. S. Moore, "The subterranean estuary: a reaction zone of groundwater and sea water," *Marine Chemistry*, vol. 65, pp. 111-125, 1999.

[8] D. G. Capone, and J. M. Slater, "Interannual patterns of water-table height and groundwater derived nitrate in nearshore sediments," *Biogeochemistry*, vol. 10, no. 3, pp. 277-288, 1990.

[9] Y. Uchiyama, K. Nadaoka, P. Rolke, K. Adachi, and H. Yagi, "Submarine groundwater discharge into the sea and associated nutrient transport in a sandy beach," *Water Resources Research*, vol. 36, no. 6, pp. 1467-1479, 2000.

[10] M. A. Charette, and E. R. Sholkovitz, "Oxidative precipitation of groundwater-derived ferrous iron in the subterranean estuary of a coastal bay," *Geophysical Research Letters*, vol. 29, 2002. art. no.-1444.

[11] S. Ueda, U. G. Chun-Sim, M. Suzumura, and E. Sumi, "Denitrification in a seashore sandy deposit influenced by groundwater discharge," *Biogeochemistry*, vol. 63, pp. 187-205, 2003

[12] V. Nyvang, "Redox processes at the salt-/freshwater interface in an anaerobic aquifer," Ph. D. dissertation, Technical University of Denmark, 2003.

[13] D. R. Aguilera, P. Jourabchi, C. Spiteri, and P. Regnier, "A knowledge-based reactive transport approach for the simulation of biogeochemical dynamics in earth systems," *Geochemistry, Geophysics and Geosystems*, vol. 6, 2005, (Q07012, doi: 10 1029/2004GC000899).

[14] A. Scheidegger, "General Theory of Dispersion in Porous Media," *Journal of Geophysical Research*, vol. 66, no.10, pp. 3273, 1961.

[15] C. Meile and K. Tuncay, "Scale dependence of reaction rates in porous media," *Advances in Water Resources,* vol. 29, pp. 62-71, 2006

[16] J. N. Reddy, An *introduction to the finite element method*. 2nd ed. New York: McGraw-Hill, 1993.

[17] C. Spiteri, P. Regnier, C. P. Slomp, and M. A. Charette, "pH-Dependent iron oxide precipitation in a subterranean estuary," *Journal of Geochemical Exploration*, vol. 88, pp. 399-403, 2006.

[18] J. M. Talbot, K. D. Kroeger, A. Rago, M. C. Allen, and M A. Charette, "Nitrogen flux and speciation through the subterranean estuary of Waquoit Bay, Massachusetts," *Biological Bulletin*, vol. 205, pp. 244-245, 2003.

[19] J. E. Cable, D. R. Corbett, and M. M. Walsh, "Phosphate uptake in coastal aquifers: a fresh look at wastewater management," *Limnology and Oceanography Bulletin*, vol. 11, no. 2, pp. 1-4, 2002.

[20] V. Vanek, "In situ treatment of iron-rich groundwater by addition of nitrate," Rep. Lunds Universiteit, pp. 33, 1990.

[21] S. F. Korom, "Natural denitrification in the saturated zone: A review," *Water Reseources Research*, vol. 28, no. 6, pp. 1657-1668, 1992.

[22] D. Postma, "Kinetics of nitrate by detrital Fe(II)-silicates," *Geochimica et Cosmochimica Acta*, vol. 54, pp. 903-908, 1990.

[23] E. K. Berner, and R. A. Berner, *Global Environment Water, Air and Geochemical cycles*, Prentice Hall, New Jersey, 1996, pp. 376.

[24] M. A. Charette, E. R. Sholkovitz, and Hansel C. M., "Trace elements cycling in a subterranean estuary: Part 1. Geochemistry of the permeable sediments," *Geochimica et Cosmochimica Acta*, vol. 69, no. 8, pp. 2095-2109, 2005.

[25] P. Van Cappellen, and Y. Wang, "Metal cycling in surface sediments: modeling the interplay of transport and reaction," in *Metal Contaminated Sediments*, H.E. Allen Ed. Ann Arbor Press, Chelsea, Michigan, 1995, pp. 21-62.

[26] M. D. Krom, and R. A. Berner, "Adsorption of phosphate in anoxic marine sediments," *Limnology and Oceanography*, vol. 25, no. 5, pp. 797-806, 1980.

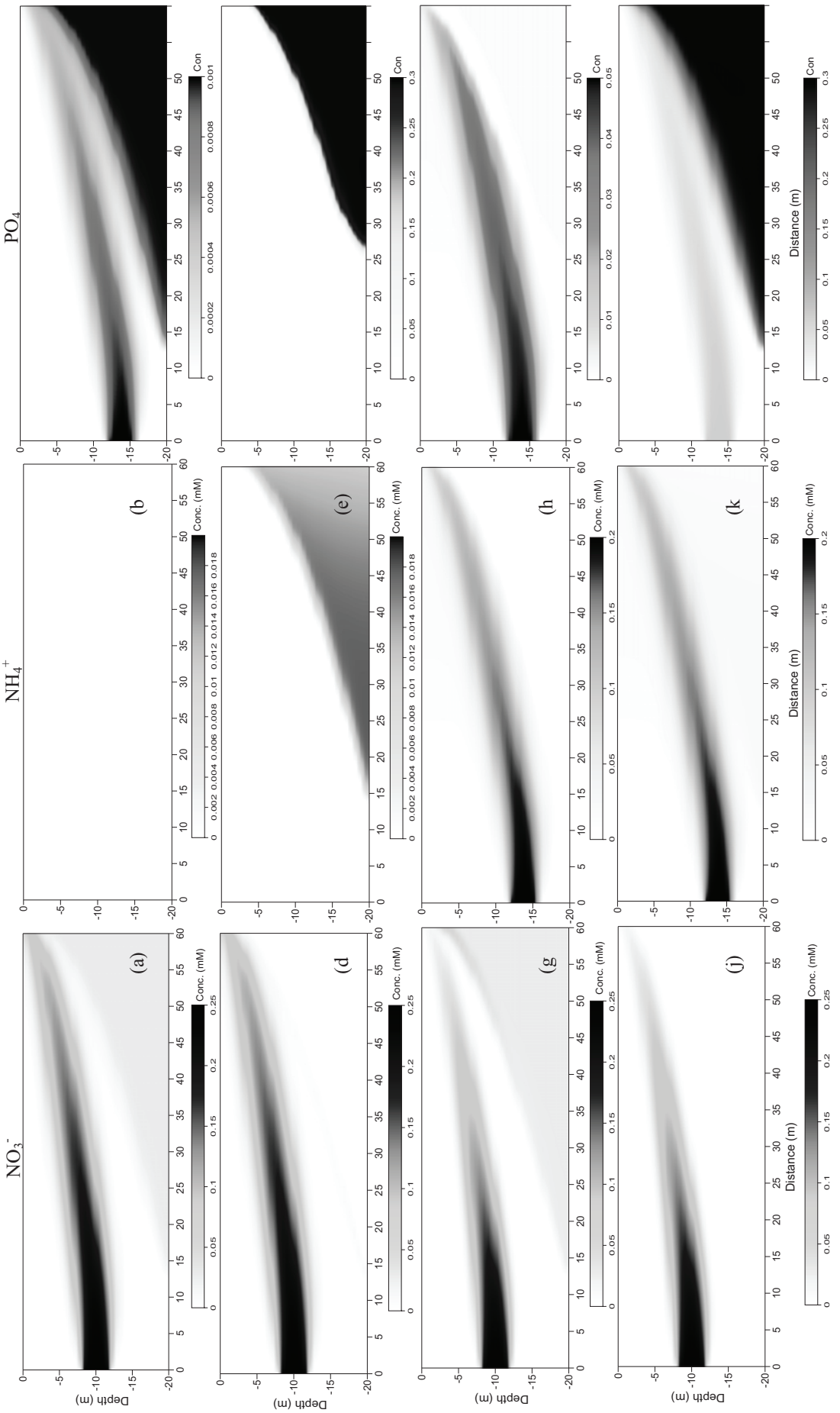

Fig 3 Simulated 2D steady-state distributions for NO_3^-, NH_4^+ and PO_4 obtained for Case 1 (oxic groundwater-oxic seawater), Case 2 (oxic groundwater-anoxic seawater), Case 3 (anoxic groundwater-oxic seawater) and Case 4 (anoxic groundwater-anoxic seawater

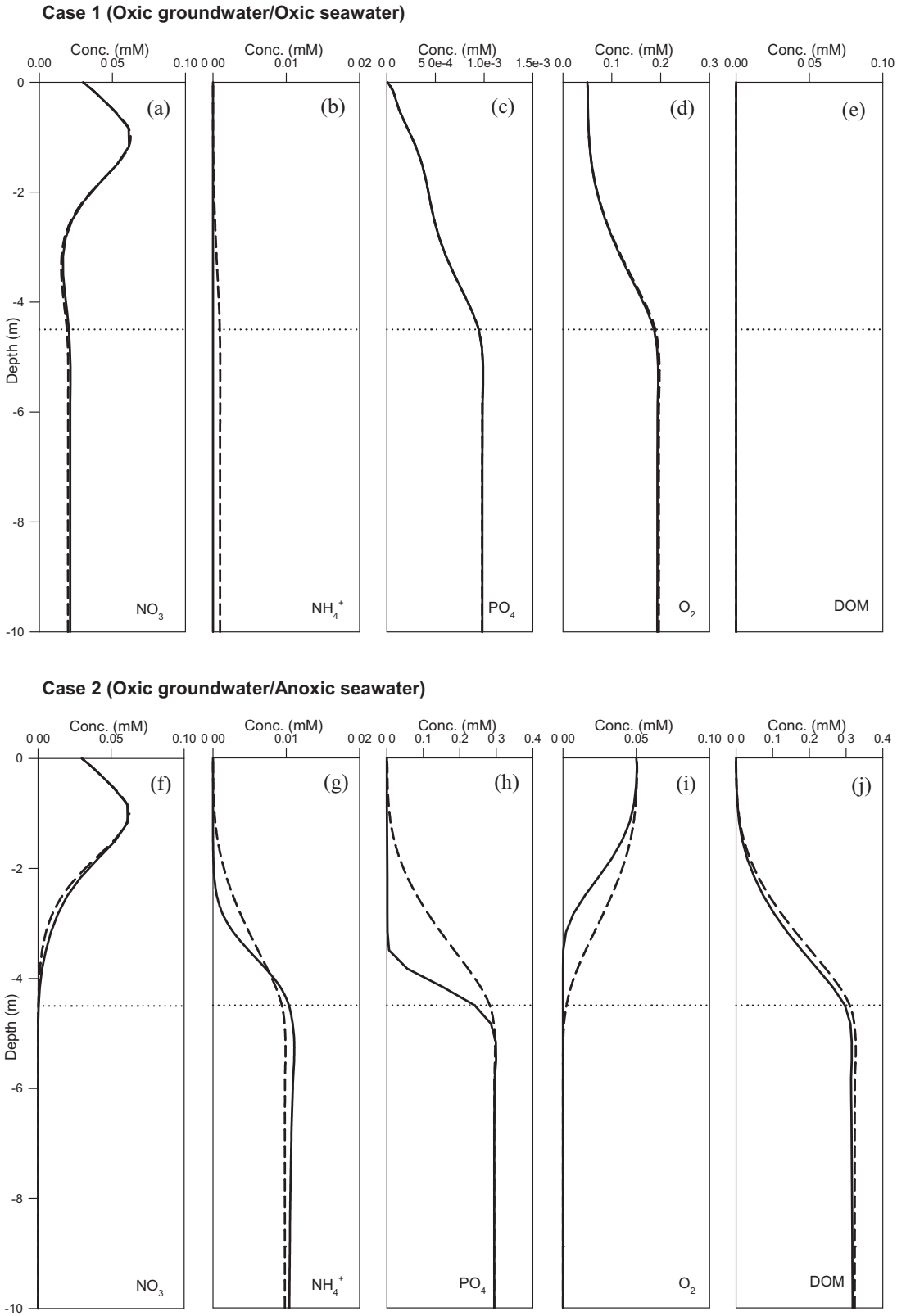
Case 1 (Oxic groundwater/Oxic seawater)
Conc. (mM)
0.00
0 05
0.10
(a)
NO3
0 00
0.01
0 02
(b)
NH4+
0 0
5 0e-4
1.0e-3
1.5e-3
(c)
PO4
0.0
0.1
0.2
0.3
(d)
O2
0.00
0 05
0.10
(e)
DOM
Depth (m)
0
-2
-4
-6
-8
-10
Case 2 (Oxic groundwater/Anoxic seawater)
0 00
0.05
0.10
(f)
NO3
0 00
0.01
0 02
(g)
NH4+
0 0
0.1
0.2
0 3
0.4
(h)
PO4
0 00
0.05
0.10
(i)
O2
0 0
0.1
0.2
0 3
0.4
(j)
DOM
Depth (m)

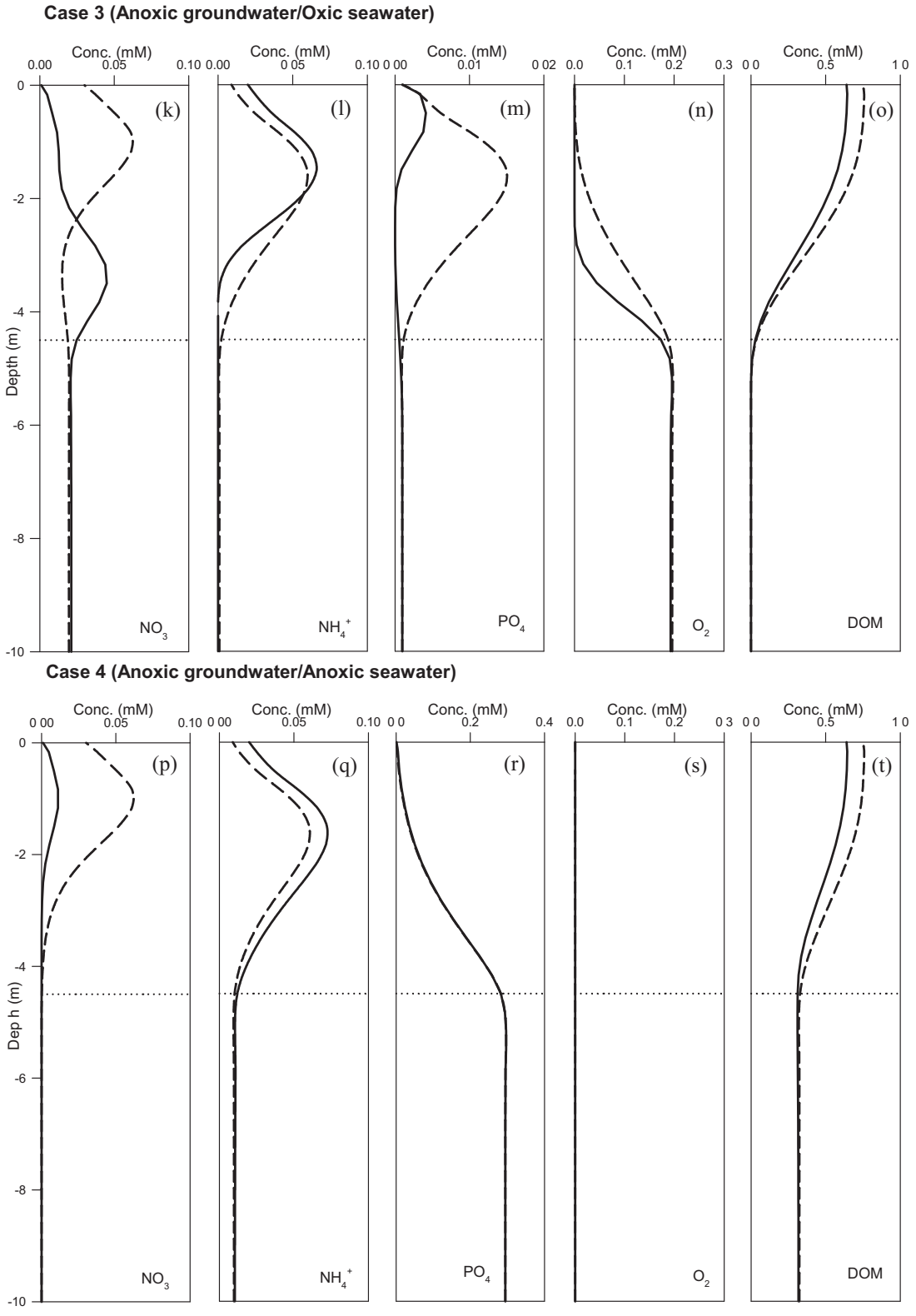

Fig. 4. NO_3, NH_4^+, PO_4, O_2 and DOM concentration profiles at the seaward boundary for the top 10 m depth (solid lines), compared with their respective conservative profiles (dashed lines). The horizontal dotted line indicates the freshwater-seawater interface, based on the modeled salinity.

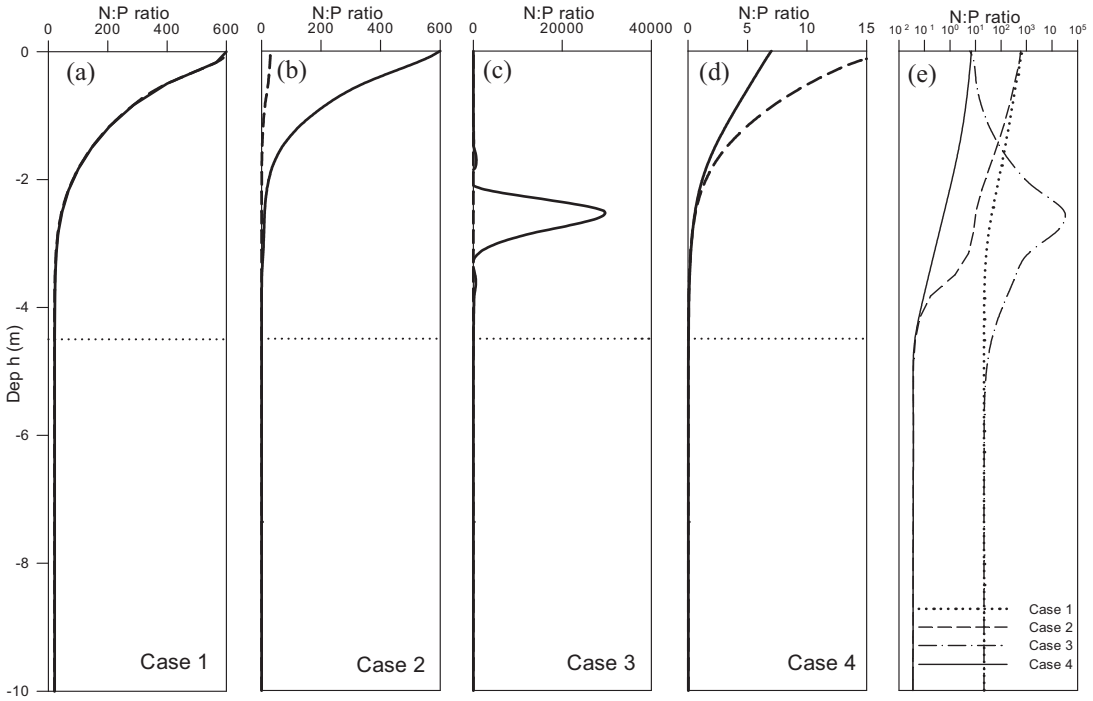

Fig. 5. Simulated N:P profiles for Cases 1-4 (solid lines, panels a-d), together with the respective profiles obtained in conservative runs (dashed lines) over the top 10 m. Note that the x-axis of panel e) is on a logarithmic scale. The horizontal dotted line indicates the freshwater-seawater interface, based on the modeled salinity

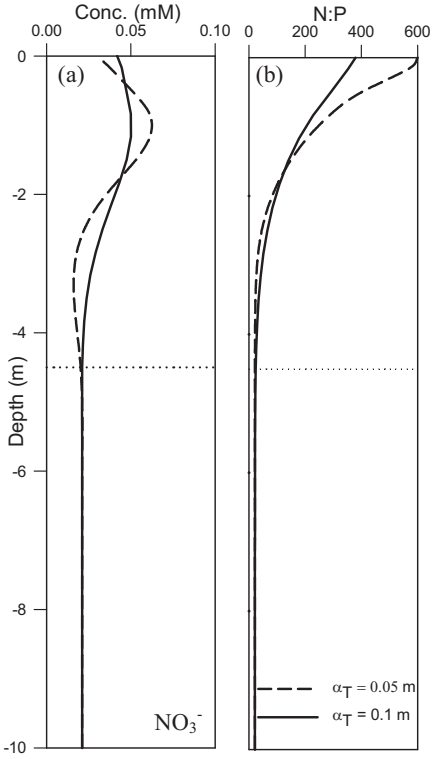

Fig. 6. Profiles of NO3- (a) and N:P ratio (b) over the top 10 m on the seawat boundary obtained with αT 0.1 m, compared to the baseline profiles with an αT 0.05 m (Case 1). The horizontal dotted line indicates the freshwater-seawater interface, based on the modeled salinity.

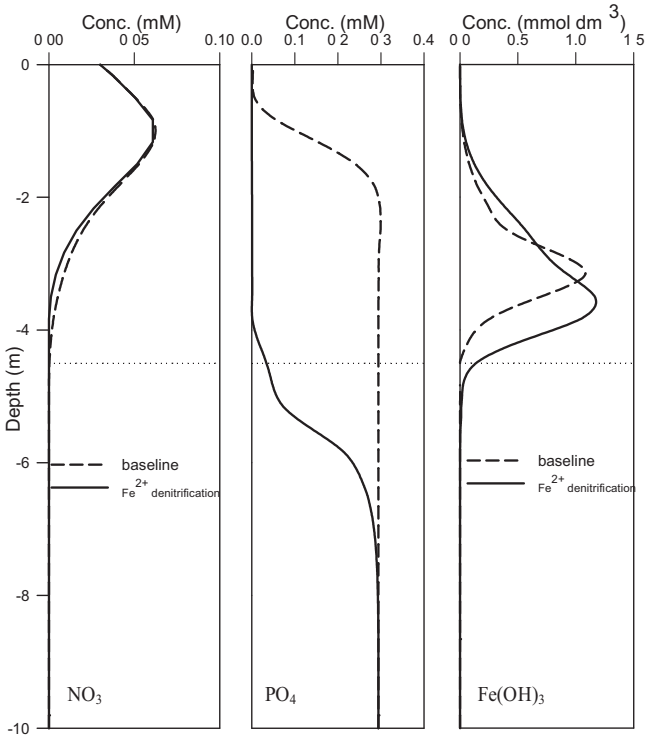

Fig. 7. Profiles of NO_3 (a), PO_4 (b) and $Fe(OH)_3$ (c) over the top 10 m, obtained when Fe^{2+} denitrification is included in the reaction network (solid lines), compared to the baseline profiles (dashed lines) (Case 2). The horizontal dotted line indicates the freshwater-seawater interface, based on the modeled salinity.

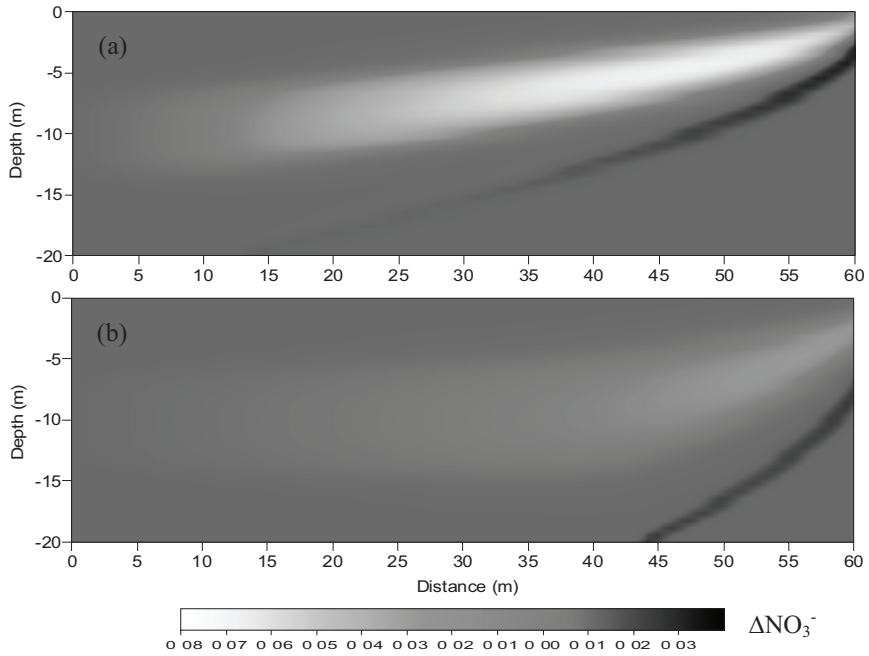

Fig. 8. Difference in NO_3 concentrations for Case 3 (mM) (a) between baseline and conservative run, with a groundwaterhead of 0.4 m and (b) sensitivity run 3 and corresponding conservative run with a groundwater head of 0.8 m, simulating higher water flow velocity.

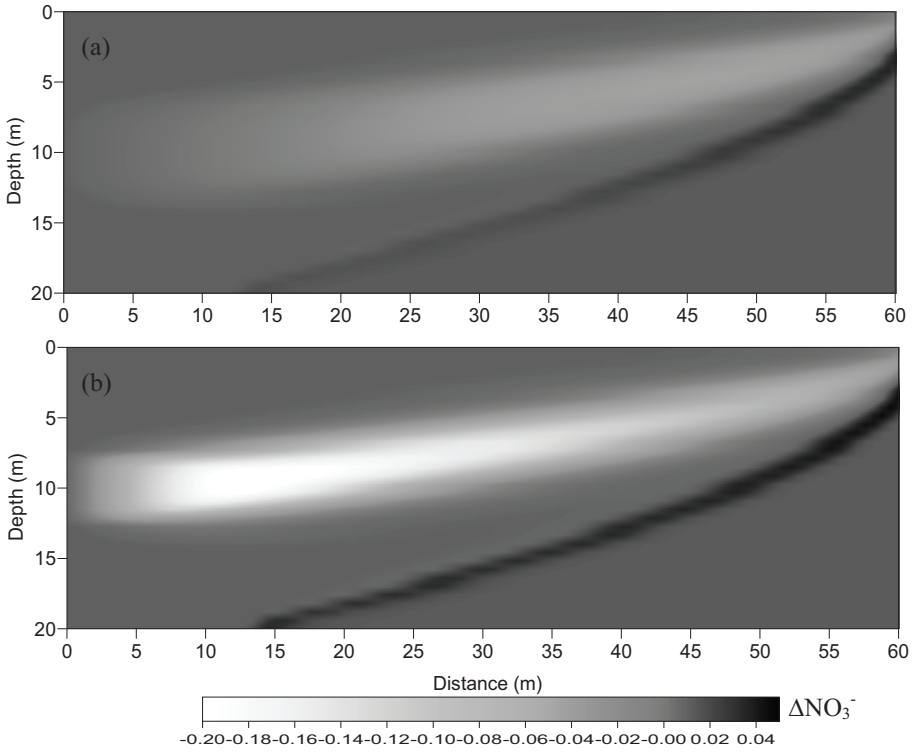

Fig. 9. Difference in NO_3 concentrations (mM) for Case 3 (a) between baseline and conservative run (identical to Fig. 8a above but plotted on a different scale) and (b) sensitivity run 4 (k_{fox} 3.0 x 10^{8} s^{1}; Table 4) and corresponding conservative run.

TABLE 2
THE REACTION NETWORK AND KINETIC FORMULATIONS USED IN THE MODEL

Name	Reaction	Kinetic formulation
Reaction network used in "Base simulations"		
Oxic degradation	$CH_2O^* + xO_2 + (-y+2z)HCO_3^- \rightarrow (x-y+2z)CO_2 + yNH_4 + zHPO_4^{2-} + (x-y+2z)H_2O$	If $O_2 > kmo2$; Rate = $kf_{ox}[CH_2O]$ If $O_2 < kmo2$; Rate = $kf_{ox}[CH_2O]\frac{[O_2]}{kmo2}$
Denitrification	$CH_2O + 0.8xNO_3^- \rightarrow 0.4xN_2 + (0.2x-y+2z)CO_2 + (0.8x+y-2z)HCO_3^- + yNH_4 + zHPO_4^{2-} + (0.6x-y+2z)H_2O$	If $O_2 > kmo2$; Rate = 0 If $O_2 < kmo2$ and $NO_3^- > kmno3$; Rate = $kf_{ox}[CH_2O]\left(1-\frac{[O_2]}{kmo2}\right)$ If $O_2 < kmo2$ and $NO_3^- < kmno3$; Rate = $kf_{ox}[CH_2O]\left(1-\frac{[O_2]}{kmo2}\right)\frac{[NO_3^-]}{kmno3}$
$Fe(OH)_3$ reduction	$CH_2O + 4xFe(OH)_3 + (7x+y-2z)CO_2 \rightarrow 4xFe^{2+} + (8x+y-2z)HCO_3^- + yNH_4 + zHPO_4^{2-} + (3x-y+2z)H_2O$	If $NO_3^- > kmno3$; Rate = 0 If $NO_3^- < kmno3$ and $Fe(OH)_3 > kmfe$; Rate = $kf_{ox}[CH_2O]\left(1-\frac{[O_2]}{kmo2}-\frac{[NO_3^-]}{kmno3}\right)$ If $NO_3^- < kmno3$ and $Fe(OH)_3 < kmfe$; Rate = $kf_{ox}[CH_2O]\left(1-\frac{[O_2]}{kmo2}-\frac{[NO_3^-]}{kmno3}\right)\frac{[Fe(OH)}{kmfe}$
Nitrification	$NH_4 + 2O_2 + 2HCO_3^- \rightarrow NO_3^- + 2CO_2 + 3H_2O$	Rate = $k_{nitri}[NH_4^+][O_2]$
Fe^{2+} reoxidation	$Fe^{2+} + 0.25O_2 + 2HCO_3^- + 0.5H_2O \rightarrow Fe(OH)_3 + 2CO_2$	Rate = $k_{feox}[Fe^{2+}][O_2]$
Extended reaction network used in "Sensitivity Analysis"		
Denitrification via Fe^{2+}	$5Fe^{2+} + NO_3^- + 12H_2O \rightarrow 5Fe(OH)_3 + 0.5N_2 + 9H$	Rate = $k_{feno3}[Fe^{2+}][NO_3^-]$

* $CH_2O=(CH_2O)x(NH_3)_y(H_3PO_4)_z$, where x, y, z represent the C:N:P ratios, set as 106:11:1 for coastal environments [25]

TABLE 3
REACTION PARAMETER VALUES USED IN THE MODEL

Parameter (units)	Description	Value
kf_{ox} (s^{-1})	Rate constant for decomposition of DOM	3.0×10^{-9} [a]
k_{nitri} ($mM^{-1}\ s^{-1}$)	Rate constant for nitrification	4.8×10^{-4} [a]
k_{feox} ($mM^{-1}\ s^{-1}$)	Rate constant for Fe^{2+} reoxidation	6.4×10^{-2} [a]
k_{feno3} ($mM^{-1}\ s^{-1}$)	Rate constant for Fe^{2+} denitrification	6.4×10^{-2} [b]
kmo2 (mM)	Limiting concentration of O_2	0.008 [a]
kmno3 (mM)	Limiting concentration of NO_3^-	0.001 [a]
kmfe (mmol dm^{-3})	Limiting concentration of $Fe(OH)_3$	18.95 [a]
K ($dm^3\ mmol^{-1}$)	Adsorption coefficient for PO_4 adsorption	1545 [c]

a [25]; b assumed to be equal to Fe^{2+} reoxidation with O_2; c calculated assuming a $Fe(OH)_3$ concentration of 0.2 mmol dm^{-3} and a dimensionless K_d of 309 [26]

TABLE 4
LIST OF SENSITIVITY ANALYSIS RUNS

Run Number	Case	Parameter changed/reaction added	Aim
1	1	$\alpha_T = 0.1$ m	To assess the effect of α_T on the extent of freshwater/seawater mixing
2	2	Denitrification via Fe^{2+}	To assess the additional NO_3^- removal potential using Fe(II) as the electron donor
3	3	Freshwater head = 0.8 m	To test the effect of flow rate on denitrification
4	3	kfox = 3.0×10^{-8} s^{-1}	To test the effect of DOM reactivity on NO_3 removal